AO07: Temporal variability of surface albedo

Supervisors: Dr R.G. Grainger, Mr A.M. Sayer
Candidate no. 46666, Word count: 7587

Abstract

This study aims to assess the validity of using a mean surface albedo renewed every 8 days (MODIS) as the *a priori* data in the retrieval of daily aerosol properties from AATSR. Estimates of the likely 8-day variability within the averaged albedos were made for different surface types and these were grouped into three broad categories: snowy, bare or vegetated. Where significant temporal variation was found additional error terms were included in the aerosol retrieval and a comparison was made with the current scheme. It was found that going some way to accounting for the temporal variability within 8-day periods improved the aerosol retrieval. The proportion of retrievals converging at low cost increased from around 70% to 85% and there was better agreement with ground-based measurements (R increased from 0.74 to 0.85). The improved retrieval scheme suggests a larger optical depth than the current scheme.

1 Introduction

Accurately quantifying the abundance and distribution of aerosols is a highly relevant problem. Compared to greenhouse gases relatively little is known about their forcing effects on the climate. Effects can either be direct: aerosol particles scatter or absorb shortwave radiation themselves, or indirect: they change cloud cover and cloud properties thus altering the Earth's albedo. Estimates of the radiative forcing due to aerosol direct effects range between -0.1 and -0.9 W m^{-2} (Solomon et al., 2007) and are even less precisely known for indirect effects, lying somewhere between -0.3 and -1.8 W m^{-2} for cloud albedo effects (Solomon et al., 2007) and -0.5 and -1.9 W m^{-2} for cloud lifetime effects (Lohmann and Feichter, 2005). This is an area that needs to be explored to get a better idea of the likelihood of different climate change scenarios and a good dataset is demanded by models.

To perform useful aerosol retrievals using the method of remote sensing, an accurate description of the surface reflectance is needed. The satellite radiometer (here the focus is specifically on the Advanced Along-Track Scanning Radiometer, AATSR) measures the top-of-atmosphere (TOA) radiance which primarily consists of light reflected from the Earth's surface altered slightly by atmospheric aerosols. In most cases, the aerosols provide only a small perturbation from which the optical depth and abundance can be deduced using retrieval theory. The Oxford-RAL Aerosol and Cloud (ORAC) retrieval scheme is used here, which requires *a priori* data that must be a realistic and accurate representation of the true surface state. For the ORAC scheme, the Moderate Resolution Imaging Spectroradiometer

(MODIS) provides this information currently using 16 days of observations to produce a mean surface albedo every 8 days. However, from simple day-to-day observations it is clear that the optical properties of the ground can change much more rapidly, for example due to rain dampening and darkening soil, a covering of highly reflective snow, or sudden changes in vegetation. According to Sellers (1993) an absolute accuracy of 0.02 in the land surface albedo is needed for use in climate models. If the true value of the surface albedo deviates from the 8-day mean by more than this then the aerosol retrieval may not be reliable. This investigation looks at the various ways in which the albedo could change on timescales less than 8-days and where significant deviations from the currently used MODIS product (MCD43B1) are found, more realistic error estimates on the *a priori* data are fed into the retrieval model with intention of obtaining an improved aerosol dataset.

Although the main motivation for this study is to improve, or at least ascertain, the validity of aerosol retrievals, the variation in surface albedo is important in its own right as it determines the energy balance at the surface. In addition, better understanding could lead to practical applications for monitoring land use changes using remote sensing to detect deforestation or wind erosion for example (Chappell et al., 2006).

The following section gives an overview of the retrieval processes used for the surface reflectance and aerosol parameters. Then some relevant literature is discussed as a background to this study. Section 2 describes the method and justifies the variability error estimates decided upon. An assessment of the retrieval performed with these adjusted errors is presented in Section 3.

1.1 Retrieval processes

In atmospheric physics it is often easier to measure one or more quantities related to the desired variable rather than that variable itself. The method of inverting the collected measurements to extract the state of the system is known as retrieval theory. Usually this involves more information than the measurements alone - uncertainties and the previous state of the system (*a priori* data) can be taken into account and appropriately weighted in order to refine the output and better constrain its error estimates.

1.1.1 BRDF retrieval

The bidirectional reflectance distribution function (BRDF) models the reflectance of a surface as a function of the illumination and viewing angles, and depends on the wavelength of light and the optical properties and structure of the surface. The MODIS sensors on board NASA's Earth Observing System (EOS) receive TOA radiance in 36 spectral bands, 4 of which are used here: 550, 660, 870 and 1600 nm. The TOA radiance is quality controlled (e.g. cloudy pixels are removed) and atmospherically corrected and then used to calculate the surface BRDF of the Earth. A kernel-driven model is employed based on three types of scattering: isotropic, volumetric (due to gaps between small scale structures e.g. leaves) and geometric (due to gaps between larger structures e.g. trees). For derivations of the kernels see Wanner et al. (1995) and Lucht et al. (2000).

The albedo is defined as the ratio of the upwelling to downwelling flux of solar radiation at the Earth's surface. It might be expected to depend on viewing geometry, illumination geometry, the surface optical properties and any surface structure. By integrating the BRDF with respect to view angle and relative azimuth angle, a quantity known as the black-sky albedo is obtained. This is equivalent to the albedo when there is no diffuse downwelling flux. If the black-sky albedo is integrated over solar angle, the white-sky albedo is produced which is the albedo when there is no direct downwelling flux and the diffuse component is isotropic. To reach the actual albedo (blue-sky albedo) the mean is calculated, weighted by the proportion of diffuse radiation.

The MCD43B1 data consists of the weighting parameters in the BRDF so the white-sky albedo can be obtained following the steps described above for each of the instrument channels: 550, 660, 870 and 1600 nm. (In this report the term albedo should be taken to mean the white-sky albedo at each wavelength.) 16 days of observations are used to produce each albedo value, repeated every 8 days. The justification for this period is to ensure there is sufficient cloud-free data and the different overpasses look at the BRDF from different angles. It has been assumed that the surface does not change substantially over this period - we aim to check that assumption here. The albedos plus their associated errors are fed into the ORAC retrieval scheme which delivers the aerosol optical depth, effective radius and white-sky albedo at each channel.

1.1.2 ORAC retrieval

In order to obtain the aerosol parameters from the surface reflectance (MODIS) and TOA reflectance (AATSR) measurements, a radiative transfer model is used to separate the surface and atmospheric contributions. The ORAC algorithm is an optimal estimation process that performs this task. Optimal estimation maximises the probability that the system is in the retrieved state, making use of measurement uncertainties and *a priori* data as a guide towards the most likely solution. One way of doing this is to minimise the cost function - the sum of deviations from the measured state, *a priori* state and parameters of the model weighted by the associated errors. The required elements of the aerosol retrieval *a priori* covariance matrix consist of the products of the errors at each pair of wavelengths and the correlations between them. The possible errors include:

- MODIS quoted errors due to instrument noise and systematic errors. At present 0.02 is used; this is adjusted to 10% with a minimum of 0.005 in the new error scheme developed here.

- Visible channel filter shape errors (or SVD errors) arising out of the statistical fitting method used to match MODIS and AATSR channel response functions. Sayer (2008) gives details.

- Errors due to the real temporal variation of the surface albedo ignored by using the mean over 8 days (denoted T_{8ij}). This study aims to quantify these by looking at the variability between 8-day periods (Section 2.1).

- Variations caused by diurnal cycles (denoted T_{1ij}) i.e. are there significant differences throughout the day such that the MODIS and AATSR albedos cannot be directly compared? This is addressed in Section 2.2 using published literature.

1.2 Motivation for study

According to Stroeve et al. (2006) the 16-day time frame is too coarse to precisely resolve fundamental changes at the surface, such as snow, rain, frost and

the effect of wind on the local landscape. The extent to which the daily albedo deviates from the mean will depend on the surface type: Pinter Jr. (1986) finds that dew leads to an increase in albedo over vegetation, whereas Wheeler et al. (1994) show a decrease over alkali flats in New Mexico. Even within soil types the sign of the change can vary, e.g. in response to rainfall (Chappell et al., 2006).

The polar regions are a good place to begin, since the positive feedback processes are fairly intuitive: snowmelt decreases the albedo, meaning less reflection and more absorption of radiation at the surface, hence yet more melting so the albedo decreases further. Changes over the summer months can be dramatic. Perovich et al. (2002) present a comprehensive study in the Arctic and quote broadband albedo values as disparate as 0.1 for the deepest melt ponds and 0.9 over freshly fallen snow in the same spatial area within a few months. A lot of physics is going on during this period as the surface varies greatly, yet it is all supposedly encompassed within a few MODIS mean albedo values. (Although the MODIS albedos are spectral, looking at published figures for broadband albedo gives an idea of the probable magnitudes of variability and the timescales involved.) By early June, the increased insolation and warmer weather has caused some initial melting, lowering the albedo from about 0.85 for cold snow covering ice to 0.72 for wet snow. In mid-June, melt ponds with albedos of approximately 0.3 were common; and this value decreased as low as about 0.1 as the ponds deepened in late July. Although intermediate bare ice means the average albedo of the area would not fall as low as this, 50% reductions over about 4 months were common. The summer transition period can be divided into five sections (Perovich et al., 2002) the shortest of which - pond formation - can be only a week long and corresponded to a sudden decrease in albedo from 0.7 to 0.5. This seems a worryingly large change over only half of the period used by MODIS to construct their average 8-day value.

Sharp drops can be seen over even shorter timescales - from day-to-day if caused by local weather conditions. Perovich et al. (2002) report a 0.05-0.15 decrease in albedo as a result of rain wetting previously dry snow. Ehn et al. (2006) present similar findings attributed to rain and warm weather, and quote an albedo decrease rate of -0.047 per day over 5 days. Considering the size of the MODIS errors (0.02 or 10%) this could be a major problem. Conversely, fresh snowfall or refreezing produces a sudden rise in albedo. The underlying surface is less important for opaque coverings such as snow or very heavy frost than it is for rain, but obviously the magnitude of the

albedo change would be greater if snow fell on dark soil compared to light soil. If this is not input correctly into the retrieval scheme, the aerosol parameters obtained may be erroneous because the scheme would try to look at perturbations to incorrect radiances. The extent to which the reflectance changes depends on the coating - its depth, composition and time dependence; the underlying surface and its previous condition; and the wavelength. Possible coatings include snow, frost, dew, man-made substances (e.g. black carbon), sand or dust deposited by wind and the reciprocal effect of wind erosion removing the top layer of soil.

Frost works in much the same way as snow - a highly reflective white layer added on top of the surface raises the albedo. Black carbon would, of course, have the opposite effect since it is highly absorbing. As a precaution in their field studies Perovich et al. (2002) monitored contamination of ice by soot from their ship. The level of contamination was judged to be negligible but this may not always be the case, especially near industrial areas.

A more subtle effect is dust or sand deposition on (or removal from) an area where the underlying soil has different properties. It is well known that Saharan dust can be transported across the Atlantic to South America (Koren et al., 2006). Mineral dust is itself one of the aerosols retrieved by ORAC - with more time it would be interesting to look at the differences in optical properties of dust particles when airborne and when settled on the surface.

When combined with rain, wind erosion can contribute to a significant proportion of the variability of soil surface reflectance. Rain-splash causing a crust to form, loose material covering the crust and selective erosion removing particles of a particular composition and so colour and size all affect the roughness and optical properties of the surface and thus could change the albedo. Chappell et al. (2006) give a detailed analysis using fine soils. As expected, the results depend on the soil type.

One of the main difficulties in quantifying surface reflectance is dependence on recent conditions. For example, an hour of light rain would be expected to produce a substantial drop in albedo over light soils during a dry period, but would have a negligible effect if the underlying soil was already damp. Heavier, prolonged rain may increase the albedo once puddles start to form because the reflectance of water is greater than that of damp, darkened soils.

The variability of the surface albedo is generally very low over most of the world's hot deserts (precipitation is rare) but torrential rains in Australia in 2001 were responsible for a significant albedo de-
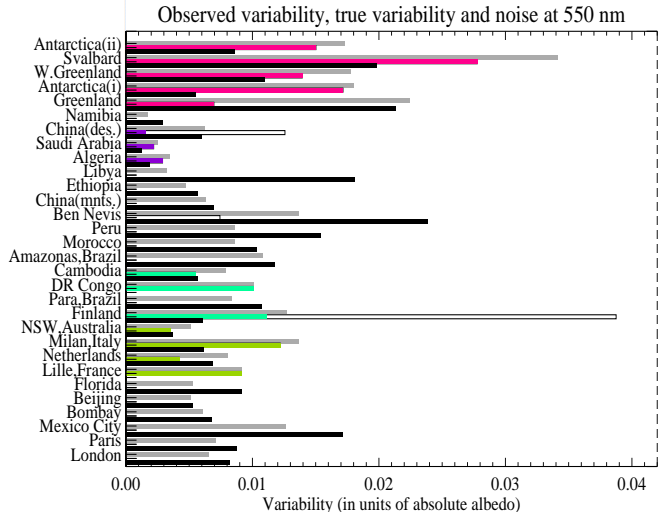
Figure 1: Bar plot showing the observed variability (grey), noise (black) and estimated true variability (coloured) in albedo at 550 nm for each location, grouped by surface type. Outlined bars show variability estimates before the removal of uncharacteristic snowy times. Data for the other channels can be found in the Appendix, Table 4.

crease (Tsvetsinskaya et al., 2006). Notably, this was a big enough signal that it is identifiable from a 16-day mean.

Finally we consider the albedo of vegetated areas. Strong seasonal variation can be seen by eye as bare trees develop leaves, green-up occurs, flowers bloom, followed by reds in autumn through to senescence. At least for the visible spectrum the phenological cycle is evident in the albedo measurements (Figure 7 in the Appendix). A study in West Africa (Oguntunde and van de Giesen, 2004) obtained the following values for the mean albedo over maize: at emergence (0.179), flowering (0.270) and maturity (0.276). Generally the seasonal variation in albedo is smooth and on large enough scales to be identified in plots of the bi-monthly mean (Jin et al., 2003). However this may not always be the case, for example when gales blow all the leaves off trees overnight, or areas with particularly short seasons may be less well-modelled.

2   Method

By looking at the change in the MODIS reported albedo from one 8-day average to the next, information can be gleaned about how the albedo fluctuates around the mean within the 8 days. The mean may be offset by a systematic error (e.g. due to inaccurate calibration); the fluctuations will be partly caused by other MODIS instrument errors (random noise) and partly due to real variations in the reflectivity of the

Earth's surface. For a particular location, the value of the 8-day albedo minus the previous 8-day albedo will be a combination of random noise and real variation in time - this combination is referred to as the 'observed variability' or T_{obs}. It has been assumed that any systematic error will be of the form of a constant offset and so would cancel out when considering the difference between albedos. An estimation of the actual variability (T_8) of the surface can therefore be obtained by subtracting (in quadrature) the noise (denoted T_{noise}) from the observed variability.

$$(T_8)^2 = (T_{obs})^2 - (T_{noise})^2 \qquad (1)$$

Six surface types were investigated: snow, desert, mountains, trees, crops and cities. For each type, 5 sample locations from different areas of the globe (Table 4 of the Appendix) were selected based on the availability of MODIS data and the homogeneity of the location at a scale of 10 km (judged using Google Earth (Google, 2009)). All MODIS data points within a 10×10 km box at each chosen location were averaged to give the mean albedo for each wavelength at that location. A scale of 10 km is chosen so that AATSR's forward and nadir views are in good agreement (over 90% of forward view pixels are colocated with their nadir view pixel). This spatial averaging, or superpixelling, reduces the processing time for the ORAC retrieval and so the *a priori* MODIS data only needs to be known to the resolution of a superpixel. Moreover, superpixelling the MODIS data effectively gives a larger sample size than using a single point and enables the noise to be estimated. Under the assumption of homogeneity, all pixels within the superpixel should have the same albedo at any given time but there will be some spread in the measured values as there is noise associated with the measurement. In reality, most locations will show some spatial variability. Attempting to select the least spatially variable superpixels should minimise the masking of temporal variability by spatial variability and give an idea of the minimum noise values for each surface type. Of course, examples are easier to find in Antarctica or desert compared to farmland or cities, for example. Hence the standard error on the albedo values within the superpixel can be taken as a measure of the random noise (with a spatial noise contribution too). The standard error was multiplied by a factor $\sqrt{2}$ to convert the error on the albedo measurement to the error on the variability (a difference of 2 measurements). This noise and the observed variability were averaged over 7 years of data (2002-2008) to maximise the sample sizes and reduce the impact of any atypical data. Using Equation 1, estimates of the true variability in surface albedo for each loca-
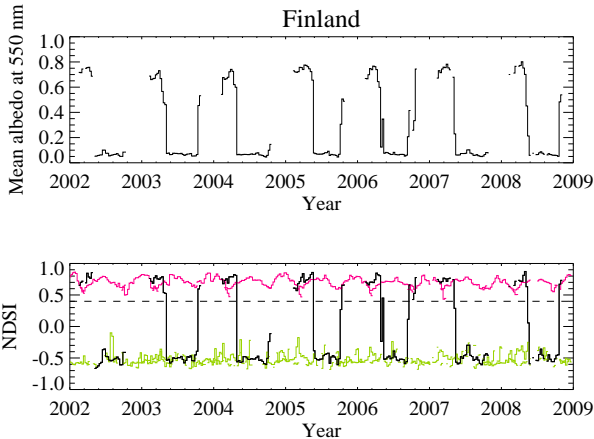
Figure 2: Time-series plots showing annual snowfall in Finland. Snow melts every April causing a sudden albedo decrease (top plot). The lower plot shows that during the winter months the NDSI (normalised difference snow index) agrees with typical values for polar regions shown in pink (Antarctica and Greenland) and after snowmelt the NDSI is much more typical of tree covered surfaces shown in green (Democratic Republic of Congo and Mekong, Cambodia). The 0.4 threshold is marked by the dashed line.
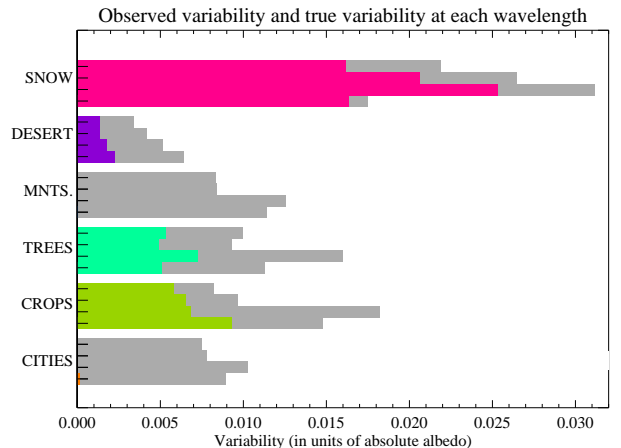

Figure 3: Bar plot showing estimates of temporal variability grouped by surface type. Each set of 4 bars corresponds to the 4 channels (from top to bottom): 550, 660, 870 and 1600 nm. Grey bars are the observed variability between 8-day periods, coloured bars are the estimated true surface variability.

tion were obtained. The coloured bars in Figure 1 show these variability estimates at 550 nm. At a glance they are of the order of 0.01, which is comparable to the errors given by MODIS and therefore need to be taken into consideration. For locations where the noise is greater than the observed variability, no coloured bars are shown, indicating that there is no need to include an additional error term specifically for temporal variations, as any changes in time are overshadowed by spatial variations and instrument noise errors. For snow, crops and trees, and to a lesser extent deserts, an appreciable portion of the observed variability is attributed to real temporal variation of the surface. This suggests that the current errors used in the albedo retrieval are too small for these surfaces and so may be over-constraining the data to fit the *a priori* values, when in reality there could be a significant discrepancy between the MODIS albedo and the actual albedo on any one day.

2.1 Variability on 8-day timescales

The outlined bars on Figure 1 illustrate variabilities deduced for three locations (Finland, Ben Nevis and China (desert)) that were particularly large compared to the other locations in their respective surface types. Looking at time-series of these locations revealed annual snowfall. Seasonal (for Finland, Figure 2) or more short-lived coverings of snow dramatically change the albedo from around 0.2 to 0.8, producing a huge and uncharacteristic change in albedo

between the 8-day periods before and after snowfall (and snow melt). This was pulling up the average variability over the 7 years, yet for the remaining times the albedo and variability appear to be typical of that surface type. The decision was taken to remove the albedos at snowy times from these three locations and calculate the means and variabilities using only the data for largely snow-free times of the year. This brings the variability estimates into agreement with the other locations of the same surface types. A normalised difference snow index (NDSI) based on Klein et al. (1998) was used with a threshold of > 0.4 to indicate snow (Riggs et al., 2006). The NDSI is given in Equation 2 where a_i is the albedo at wavelength i in nm:

$$\text{NDSI} = \frac{a_{550} - a_{1600}}{a_{550} + a_{1600}} \qquad (2)$$

Figure 2 shows how this test performs: during the summer the NDSI matches that of other forested locations (green line), in winter it fits with polar regions (pink line). It therefore seems an effective way of distinguishing between snowy and non-snowy regimes.

Using the NDSI tested data and averaging over each set of 5 locations gives an estimate of the temporal variability at each wavelength for each surface type, as in Figure 3. Overall the near-IR shows more variability than the visible, with snow and trees most variable at 870 nm and desert and crops at 1600 nm.

Snow covered surfaces can be identified as the most variable by far, followed by trees and crops which show similar variability, then deserts. It therefore seems reasonable to group trees and crops together as one 'vegetated' category. The data for mountains and cities is too noisy to enable estimates of the tem-

poral variation and these surfaces will be made up of a mixture of types (vegetation, rock and bare soil, and man-made surfaces in urban areas). Cities are a special case in that they will be highly spatially variable, comprising different land uses within a small area (i.e. adjacent pixels tend to be quite different, even a single MODIS 2.5×2.5 km pixel is likely to be heterogeneous). For cities, much of the noise between pixels arises out of spatial differences rather than instrument noise, and this is significantly larger than any temporal variations.

It was decided to divide the land surface into three categories by variability and albedo: snowy, vegetated and bare. The ORAC retrieval was adjusted to include one of three additional errors at each wavelength, selected according to the category of the superpixel being considered. First the NDSI test (Equation 2) is applied and an index greater than 0.4 classifies the superpixel as snowy. For the remaining non-snowy superpixels a similar test is used: the normalised difference vegetation index (NDVI) uses the 'greenness' to distinguish between vegetation and bare soil.

$$\text{NDVI} = \frac{a_{870} - a_{660}}{a_{870} + a_{660}} \quad (3)$$

A threshold of 0.3 and above was used so that crops and trees are classed together in the vegetated category, but differ from deserts (Table 1).

The situation is more complicated for mountains. The NDVI test classes them as vegetated but looking at Figure 3 they have low (in fact zero) temporal variability so perhaps would be better grouped with deserts. This apparent inconsistency arises out of the variety of the 5 chosen mountain locations. For example, Morocco is in the desert (NDVI = 0.127), Peru is rainforest (NDVI = 0.493) and Ben Nevis is covered by a mixture of vegetation and bare rock. Also the complex shadowing in mountainous regions means the MODIS BRDF model less accurately represents the details of the surface and the local topography makes pixels fairly heterogeneous. These added complexities mean the MODIS data is likely to be more noisy and the standard deviation of points within a superpixel is high. The true temporal variability of mountains may be slightly underestimated here as it is masked by measurement difficulties.

With more time, it would be interesting to look at the variability of three classes of mountains - vegetated, bare and snowy - and compare to similar surfaces on flat ground to see the effect of hilly terrain. Here it is hoped that by addressing superpixels individually, green mountains will be treated as vegetated whilst those in desert areas will have the errors for bare surfaces applied. Since the variances on the temporal variability between surfaces in each type are

Surface	NDSI	NDVI	Category
CITIES	-0.30 ±0.03	0.30 ±0.04	bare
CROPS	-0.46 ±0.06	0.57 ±0.11	vegetated
TREES	-0.51 ±0.02	0.74 ±0.10	vegetated
MOUNTAINS	-0.40 ±0.12	0.41 ±0.19	vegetated
DESERT	-0.43 ±0.08	0.10 ±0.02	bare
SNOW	0.73 ±0.06	-0.05 ±0.02	snowy

Table 1: NDSI and NDVI with their standard deviations and the category assigned to each surface type.

Wavelength	Snowy	Vegetated	Bare
550 nm	0.0168	0.0075	0.0019
660 nm	0.0204	0.0081	0.0023
870 nm	0.0259	0.0113	0.0030
1600 nm	0.0146	0.0112	0.0039

Table 2: Estimates of the uncertainty in albedo caused by temporal variation (in units of absolute albedo). These are the T_8 errors inserted into the adjusted retrieval scheme.

large and to avoid over-constraining, the T_8 values inserted into the retrieval were deliberately chosen to be the loosest reasonable estimates. For the surface types within each category, the largest mean variability plus one standard deviation was used. The T_8 error was calculated by dividing this value by $\sqrt{2}$ to convert from an uncertainty in the variability to an uncertainty on any individual albedo measurement. Table 2 lists the values used. The ORAC algorithm requires correlation coefficients between the different instrument channels. Correlation matrices were constructed for each location and then for each surface type (see the Appendix, Table 5). Broadly speaking, these showed the expected trends, e.g strong positive correlation between 550 and 660 nm and negative correlation with 1600 nm for snow covered surfaces. However, the variances are very high and no obvious trends were identified across surface types. For simplicity and to avoid over-constraining the correlation matrices were taken to be the unit matrix.

2.2 Diurnal cycles of albedo

The solar zenith angle (SZA) governs the diurnal variation in (blue-sky) albedo. Although we are only interested in the white-sky albedo, many studies discuss blue-sky albedo and these give an indication of the processes occurring and their implications for the surface reflectance. If SZA was the only factor, then for a given surface the daily cycle would be symmetrical with respect to the SZA (i.e. AM and PM values would be coincident for equal illumination angles). Minnis et al. (1997) showed that this is not in fact the case. Over the pastures and prairies of Oklahoma, a

discrepancy of 10% was found between morning and afternoon albedo measurements at the same SZA and was attributed mainly to dew and meteorological conditions. Wheeler et al. (1994) found similar results for a desert landscape. The effects are seasonal and greatest during dry times when dew was found to cause a change in (500-600nm) albedo by as much as 30% over the course of the day. The magnitude and sign of the effect depends on wavelength: over cropland dew increases visible, decreases mid-IR and has no effect on near-IR albedo (Pinter Jr., 1986). These studies illustrate the need to consider different surfaces case by case. A light coating of dew settled on waxy leaves will add to the reflectance because water droplets have a high specular reflectance (Pinter Jr., 1986). But the condensation of water vapour from the air onto desert sand will tend to be absorbed, darkening the surface. Furthermore, meteorological conditions play a role - warm temperatures and high wind speed at the surface accelerate the evaporation process and so produce a faster evolving change as the surface dries out more quickly.

Evidently dewfall and evaporation can significantly affect the surface albedo. However, this will only really be a problem here if the dew conditions differ appreciably between times of the AATSR overpass (10:15 local solar time) and the MODIS overpasses (10:30 (Terra) and 13:30 (Aqua)). According to Pinter Jr. (1986) almost all dew is gone by 11:00. Wheeler et al. (1994) find little change for 10:00-14:00 - most change occurs by 09:30 in the majority of cases. Any errors attributable to dew would be considerably smaller then the other errors involved (10% MODIS error, for example) and so can be neglected. In support of this Minnis et al. (1997) found that when averaged over a day, diurnal asymmetry produced errors of only about 3% - it is mostly in the early morning and late evening that the asymmetry is greatest and the effect is much reduced towards the middle of the day, i.e. around the overpass times.

For polar regions, the daily freeze-thaw cycle can cause approximately 10% variability in broadband albedo over white-ice (Ehn et al., 2006). Daytime insolation and warmer surface temperatures cause changes in grain size of the composite particles and the proportion of liquid water. Reflectivity is lower for larger grains as photons must traverse more ice between chances to escape by refraction at the grain boundary so they are more likely to be absorbed (Warren, 1982). This generally gives rise to a lower daytime albedo compared to the nighttime when refreezing occurs as the temperature drops. However, these changes are over a whole day; over the 10:15-13:30 period the albedo change is much less. Perhaps

more important to consider are short-lived weather patterns, such as snowfall and rain. Ehn et al. (2006) gives a rate of change of albedo of +0.01 hr^{-1} to -0.014 hr^{-1} during the melt season. This could amount to a difference of 0.02-0.03 between AATSR and MODIS measurements and so could be problematic. Some of the variability due to meteorological conditions will be accounted for by the T_8 errors and the melt period only covers a small portion of each year (end of May to the middle of June in the Arctic (Perovich et al., 2002)). One area that has not been well addressed by this investigation is these sudden changes during snowfall and snowmelt. These are on a different timescale to that considered here and would need to be tackled differently, perhaps using twice daily data to track how the albedo varies over shorter timescales. It is assumed that the T_1 errors for snow are small in comparison to the large T_8 variability and that the physics is at least partially accounted for within the T_8 errors.

The impact of short-lived weather events over other surfaces was also considered. Rain deposits a thin film of water on the surface, which reduces diffuse reflection due to total internal reflection at the water-air interface (Ångström, 1925). Gu et al. (2000) found an albedo decrease of about 0.1-0.15 over desert and vegetation quickly dampens and darkens (by about 0.07 over grassland and around 0.09 over cropland (Liu et al., 2008)). Chappell et al. (2006) attribute a 'significant portion' of the variability of the reflectance of soil to rainfall and wind abrasion. Different soils react differently which makes this very difficult to model in sufficiently general terms for the retrieval, as the *a priori* albedo would need to identify the soil type so that the correct error could be applied - yet it is the accuracy of the *a priori* albedo itself that is mistrusted. There could be misleading aerosol retrievals on occasions when snow begins to settle shortly after 10:15 and continues through to the afternoon but such differing albedo measurements would probably produce obviously erroneous aerosol parameters and so could be removed as bad data later using a simple range check quality control. The simplicity of this solution makes it preferable to trying to introduce an average T_1 value to account for sudden snowfall.

Finally, changes specific to vegetation were considered, such as daily albedo cycles caused by flowers opening with the sun. No evidence was found on a daily timescale. Grant et al. (2000) raise an interesting contribution to diurnal asymmetry: the leaning of grass due to wilting or wind stress, which alters the alignment of the blades with the incident solar direction and could explain the shift in the position of min-

imum albedo away from the smallest SZA. Instead the minimum would be where the blades are aligned with the incident solar rays so that photons penetrate more deeply into the vegetation and so have a higher chance of absorption before they can escape (Kimes et al., 1987). This is unlikely to cause a problem here since the effect is small and only occurs over particular types of vegetation.

Although the above literature review has led to no quantitative estimates, it highlights that the timings of the overpasses alleviate many of the potential issues with diurnal variations - this would not be the case if the measurements were made earlier in the day (dew would be more problematic) or if they were separated by a longer time (weather effects would potentially become more important). In addition, the theory helps to explain how some of the 8-day variability arises. Notably, precipitation at the time of the overpasses will generally be accompanied by cloud and so will not form part of the albedo dataset as MODIS filters out cloudy pixels, whereas rainfall followed by clear skies at the overpass times will still affect the 8-day variability.

Figure 4: Scatter plots showing the correlation between AERONET and AATSR optical depth at 550 nm for the current (top) and new (bottom) retrievals. The best fit line is in red, $y = x$ is in black.

We therefore arrive at an adjusted error scheme for the aerosol retrieval, which includes the values listed in Table 2 to account for the variation in albedo from the 8-day MODIS value. One other difference from the present scheme is that the MODIS errors have been altered from the flat value of 0.02 to a more realistic 10% of the albedo with a minimum of 0.005 (Sayer and Schaaf, 2009). The adjusted retrieval applies the NDSI and NDVI tests (Equations 2 and 3) to determine the category of the land surface and hence which temporal errors to use.

The ORAC retrieval was run for one month (Sept. 2004) at locations over the globe where ground-based measurements were sufficiently coincident to compare results - within 30 minutes and 50 km (Ichoku et al., 2002) of AERONET (AErosol RObotic NETwork) stations. AERONET is a network of radiometers located across the globe providing a standard dataset of aerosol properties for comparing against satellite retrievals. For this study these pixels are all land-based, predominantly classed as vegetated with about one third of them bare. The speciated aerosol model was employed, which chooses the aerosol class with the lowest cost (Sayer, 2008). Analysis of the statistics between the currently used ORAC and the newly adjusted retrievals follows in the next section.

3 Results

3.1 Comparison with ground-based measurements

In Figure 4 the line $y = x$ (black) would indicate perfect agreement between the retrieved aerosol and AERONET data. In both cases the data suggest that AATSR slightly underestimates the AERONET observed optical depth but the new retrieval is an improvement, bringing the gradient closer to one and the offset closer to zero - i.e. the best fit line is closest to one-to-one for the retrieval with the new error estimates. Judging from the regressions, the new retrieval exhibits a stronger linear relationship: the RMSE is lower (0.094 compared to 0.127) and R increases from 0.74 (current retrieval) to 0.85 (new retrieval).

3.2 Distribution of residuals

For an ideal retrieval scheme the distribution of residuals (retrieved minus *a priori* albedo) would be Gaussian, centered on zero (implying no bias) with 68.3% of data points lying within 1 standard deviation from the mean and 99.7% within 3. In Figure 5 the residuals have been normalised by dividing by the assumed errors summed in variance space. Explicitly these
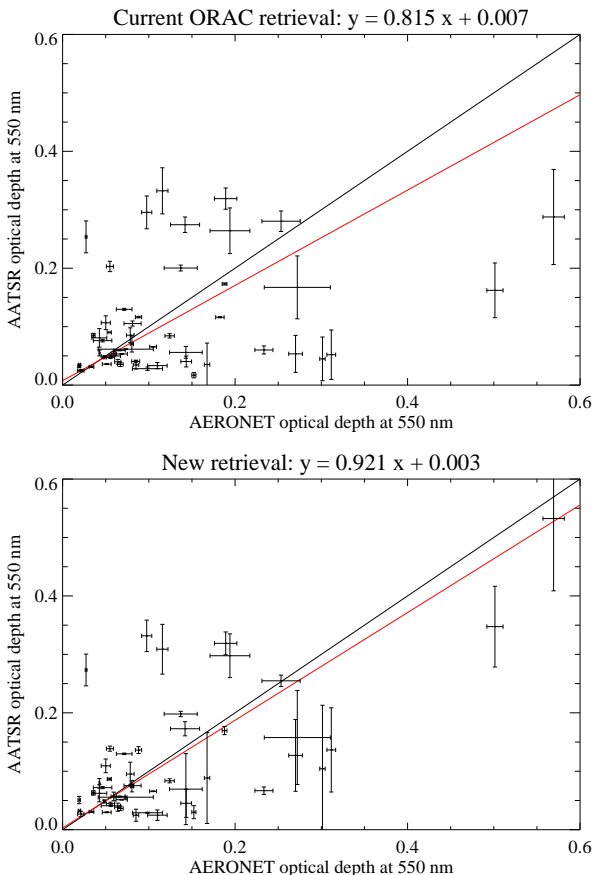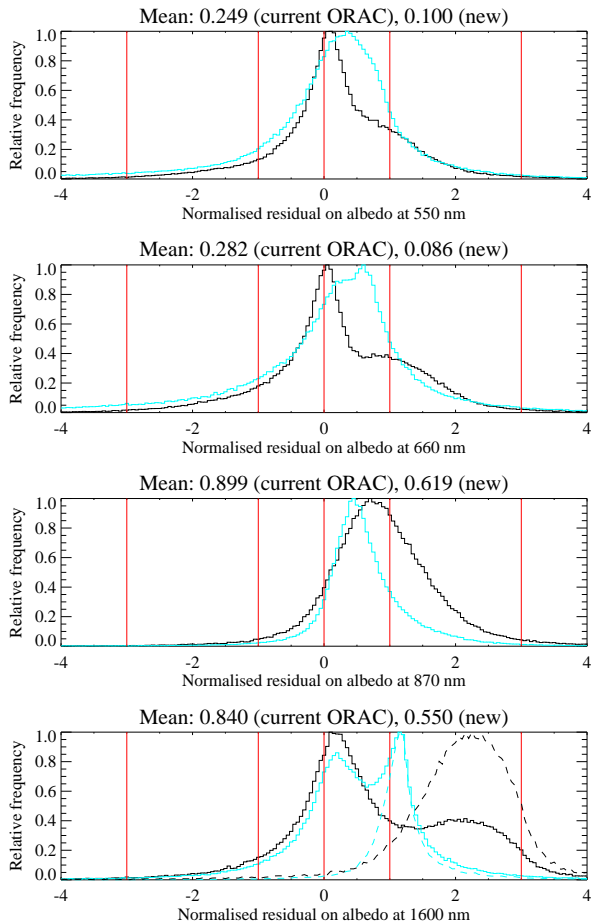
Figure 5: Normalised distributions of residuals at each wavelength. The current retrieval is shown in black; the new retrieval in blue. Vertical red lines mark the zero point, ±1 and ±3 standard deviations. At 1600 nm the dashed lines show the contributions from pixels classified as bare.

are 0.02 and SVD errors for the current retrieval, and the adjusted MODIS error, SVD errors and (category specific) temporal estimates for the new retrieval. All distributions peak at positive residual values, suggesting that the retrieved surface reflectance is on average higher than the *a priori* albedo. Pleasingly, the adjusted error scheme moves the means closer to zero for all channels. The non-adjusted data is positively skewed and there appears to be some degree of bi-modality (particularly noticeable at 660 and 1600 nm). Generally the new scheme produces a distribution that is more Gaussian in shape than the current ORAC scheme, especially at 550 and 660 nm, and goes some way to smoothing out the humps.

The bi-modality of the distributions implies two sets of residuals caused by differing regimes. These could be different surfaces, the bare and vegetated categories, with the retrieval working better over one type than over the other. The adjusted retrieval tends to sharpen the broad humps in the present data, probably because it divides the pixels into dif-ferent categories. A drawback of having only a few categories is that pixels towards the cross-over point between categories will not be particularly well represented but instead are forced into being treated either as desert or vegetation. It was found that the pixels classed as bare tend to have larger positive residuals than the vegetated pixels. When the distributions were plotted separately for these two categories, the two humps were clearly identified as vegetated (main peak) and bare (smaller, more positive peak) for both retrieval schemes. The error adjustment makes most difference for bare pixels - the looser errors sharpen the gentle bump into a narrower peak and reduce the mean residual value, i.e. bring the peak closer to the centre. This is particularly evident at 1600 nm and is shown explicitly for this channel in Figure 5. It is probably largely attributable to adjusting the MODIS errors to 10% of the albedo, since this is significant (of the order of 0.1) for deserts but much smaller for vegetation.

3.3 The cost function

The cost function is a measure of how well the retrieval works. The retrieval algorithm minimises the cost so that the probability that the system is in a given state is maximised. In theory, the mean *a priori* cost should be $5/8 = 0.625$ (from number of strong constraints/number of measurements (Sayer, 2008)) so the expected mean total cost is 1.625. For the current error scheme, the cost is high, mainly because the mean *a priori* cost is too high (0.809) suggesting that the *a priori* data is being weighted too heavily. With the adjusted scheme the mean *a priori* cost is reduced to 0.625, which matches the theoretical value (to 3 s.f.), and brings the total cost down (Table 3).

Figure 6 helps to visualise how the retrieval has been improved. The χ^2 line is a guide to how an ideal retrieval would converge - almost all data points converge quickly at low cost. In both the present and adjusted case there are more points converging at a lower cost than the χ^2 line, implying that these points generally have a loose error estimate. The adjusted retrieval is the more extreme case, as might be expected since the errors have generally been increased from the currently used 0.02 value. The looser errors give rise to the higher proportion of points converging at a lower *a priori* cost which is reflected in the total retrieval cost going down. The total cost is actually reduced too much, since the measurement cost decreases as it is not independent of the *a priori*.

On the whole, the adjusted error scheme retrieves a greater proportion of pixels accurately (about 85% compared to 70%) but less precisely than the present scheme. This means more of the retrieved values are
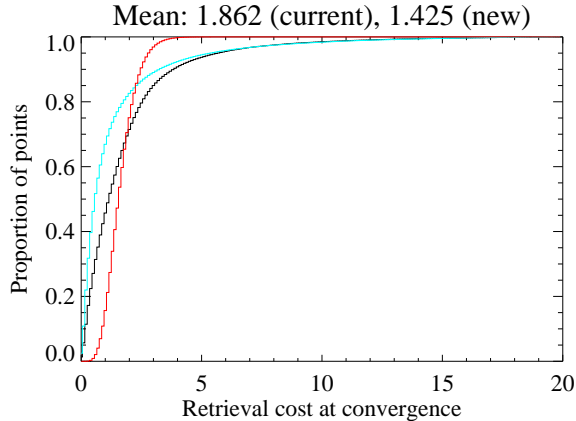
Figure 6: Cumulative distribution function of the total cost at convergence for the current (black line) and new (blue line) retrievals. The theoretical χ^2 distribution is shown in red. The plot for the *a priori* cost is very similar.

Retrieval:	Current ORAC	New errors
A priori cost	0.809	0.625
Measurement cost	1.053	0.801
Total cost	1.862	1.425

Table 3: The mean costs at convergence for different stages of the current and newly adjusted retrieval schemes.

reliable but come with larger associated uncertainties so information is still being lost, although this is partly due to the measurement cost. Importantly, the adjusted scheme decreases the number of convergences at high cost. This reduction of the distribution's tail is indicative of a higher proportion of successful retrievals.

3.4   Retrieved parameters

Generally, the retrieved parameters (optical depth at 550 nm, effective radius and surface albedo at each channel) are similar between both retrieval schemes (Appendix, Figure 8). It is reassuring that the present scheme does not appear to be producing any dramatically misleading results through a lack of consideration of temporal variability. For all parameters except the effective radius, the error estimate increases as would be expected from looking at the cost function. Interestingly, the retrieved mean optical depth increases using the adjusted scheme by 17%. Although this data only represents a small portion of the Earth's surface and is only for one month, an underestimation of the optical depth could potentially have major implications for understanding the radiative balance of the atmosphere. This extra optical depth could mean more aerosols are present in the atmosphere than AATSR currently reports, or

the aerosols are more absorbing and/or scattering at 550 nm than previously thought. Either way less solar energy is reaching the Earth's surface.

On a global scale, higher quantities of water soluble aerosols (i.e. more cloud condensation nuclei) would result in more clouds to reflect radiation back out to space, plus increased direct effects would most likely lead to an overall cooling. Conversely, extra clouds may act to trap longwave radiation and so warm the Earth. The adjusted aerosol retrieval would need to be run globally and for longer to get a better idea of possible changes to the estimated radiative forcing.

4   Conclusions

This investigation has highlighted the need for additional error terms to account for temporal variation of surface albedo not resolved by the 8-day MODIS means. Snowy surfaces were found to be the most highly variable (absolute albedo error of around 0.02) and there is a considerable amount of literature detailing changes due to weather patterns, freezing and thawing (Ehn et al., 2006; Perovich et al., 2002). On the other hand, deserts show little variability (about 0.002) supported by Tsvetsinskaya et al. (2006). Although the errors estimated here are only approximate and purposely chosen to be quite conservative, this work provides a good starting point from which to refine the method and work towards an improved retrieval. It has been seen that these looser error estimates, covering both the temporal variability and the more realistic representation of MODIS errors, give a statistically better aerosol retrieval. So far the results indicate that the optical depth may currently be being underestimated, although the new scheme would need to be applied and compared over a much larger area of the globe and for longer times.

There is huge potential for further work, mainly in improving the error estimates by looking at a larger sample of locations and other surface types, for example distinguishing between bare soil and sand, short and tall vegetation, deciduous and evergreen trees and different types of mountains. Refining the normalised difference tests and using additional thresholds to better divide the land surface into more categories should reduce the uncertainties on the estimates obtained here, enabling tighter, more suitable errors to be applied and further improvements made.

This project has achieved its aim in providing some rough values as a starting point and has shown that making some allowance for temporal variation does affect the output of the ORAC algorithm. The data is no longer being weighted as strongly to fit the *a priori* data and this gives an improved aerosol retrieval.

Acknowledgements

References

Ångström, A. (1925). The albedo of various surfaces of ground, *Geogr. Ann.* **7**.

Chappell, A., Zobeck, T. and Brunner, G. (2006). Using bi-directional soil spectral reflectance to model soil surface changes induced by rainfall and wind-tunnel abrasion, *Remote Sens. Environ.* **102**: 328–343.

Ehn, J., Granskog, M., Papakyriakou, R., Galley, R. and Barber, D. (2006). Surface albedo observations of hudson bay (canada) landfast sea ice during the spring melt, *Annals of Glaciology* **44**: 23–29.

Google (2009). *Latitude and Longitude Finder using Google Earth, Satellite Signals Limited.* http://www.satsig.net/maps/lat-long-finder.htm [Accessed 30 Jan 2009].

Grant, I., Prata, A. and Cechet, R. (2000). The impact of the diurnal variation of albedo on the remote sensing of the daily mean albedo of grassland, *J. Appl. Meteorol.* **39**: 231–244.

Gu, S., Otsuki, K. and Kamichika, M. (2000). Albedo characterstics of tottori sand dune, *J. Agric. Meteorol.* **56 (3)**.

Ichoku, C., Chu, D., Mattoo, S., Kaufman, Y., Remer, L., Tanr, D., Slutsker, I. and Holben, B. (2002). A spatio-temporal approach for global validation and analysis of modis aerosol products, *Geophys. Res. Lett.* **29**.

Jin, Y., Barker Schaaf, C., Gao, F., Li, X., Strahler, A., Lucht, W. and Liang, S. (2003). Consistency of modis surface bidirectional reflectance distribution function and albedo retrievals: 1. algorithm performance, *J. Geophys. Res.* **108**.

Kimes, D., Sellers, P. and Newcomb, W. (1987). Hemispherical reflectance variations of vegetation canopies and implications for global and regional energy budget studies, *J. Climate Appl. Meteorol.* **26**: 959–972.

Klein, A., Hall, D. and Riggs, G. (1998). Improving snow cover mapping in forests through the use of a canopy reflectance model, *Hydrol. Process.* **12**.

Koren, I., Kaufman, Y., Washington, R., Todd, M., Rudich, Y., Martins, J. and Rosenfeld, D. (2006). The bodl depression: a single spot in the sahara that provides most of the mineral dust to the amazon forests, *Environ. Res. Lett.* **1**.

Liu, H., Tu, G. and Dong, W. (2008). Three-year changes of surface albedo of degraded grassland and cropland surfaces in a semiarid area, *Chinese Science Bulletin* **53**.

Lohmann, U. and Feichter, J. (2005). Global indirect aerosol effects: a review, *Atmos. Chem. Phys.* **5**.

Lucht, W., Barker Schaaf, C. and Strahler, A. (2000). An algorithm for the retrieval of albedo from space using semiempirical brdf models, *IEEE Trans. Geosci. Remote Sensing* **38**: 977–998.

Minnis, P., Mayor, S., Smith Jr., W. and Young, D. (1997). Asymmetry in the diurnal variation of surface albedo, *IEEE Trans. Geosci. Remote Sensing* **35**: 879–891.

Oguntunde, P. and van de Giesen, N. (2004). Crop growth and development effects on surface albedo for maize and cowpea fields in ghana, west africa, *Int. J. Biometeorol.* **49**.

Perovich, D., Grenfell, T., Light, B. and Hobbs, P. (2002). Seasonal evolution of the albedo of multiyear arctic sea ice, *J. Geophys. Res.* **107**.

Pinter Jr., P. (1986). Effect of dew on canopy reflectance and temperature, *Remote Sens. Environ.* **19**: 187–205.

Riggs, G., Hall, D. and Salomonson, V. (2006). Modis snow products user guide to collection 5.

Sayer, A. (2008). *Aerosol remote sensing using AATSR*, PhD thesis, University of Oxford.

Sayer, A. and Schaaf, C. (2009). Discussion on modis error estimates, Personal communication.

Sellers, P. (1993). Remote sensing of the land surface for studies of global change, NASA/GSFC International Satellite Land Surface Climatology Project Report, Columbia MD.

Solomon, S., Qin, D., Manning, M., Marquis, M., Averyt, K., Tignor, M., Miller Jr., H. and Chen, Z. (2007). Changes in atmospheric constituents and in radiative forcing, Climate

Change 2007: the physical science basis. Contribution of Working Group 1 to the fourth assessment report of the Intergovernmental Panel on Climate Change.

Stroeve, J., Box, J. and Haran, T. (2006). Evaluation of the modis (mod10a1) daily snow albedo product over the greenland ice sheet, *Remote Sens. Environ.* **105**: 155–171.

Tsvetsinskaya, E., Barker Schaaf, C., Gao, F., Strahler, A. and Dickinson, R. (2006). Spatial and temporal variability in moderate resolution imaging spectroradiometer-derived surface albedo over global arid regions, *J. Geophys. Res.* **111**.

Wanner, W., Li, X. and Strahler, A. (1995). On the derivation of kernels for kernel-driven models of bidirectional reflectance, *J. Geophys. Res.* **100**: 21077–21089.

Warren, S. (1982). Optical properties of snow, *Rev. Geophys. Space Phys.* **20**.

Wheeler, R., LeCroy, S., Whitlock, C., Purgold, G. and Swanson, J. (1994). Surface characteristics for the alkali flats and dunes regions at white sands missile range, new mexico, *Remote Sens. Environ.* **48**.

Appendix

| | | | 550 nm | 550 nm | 550 nm | 660 nm | 660 nm | 660 nm | 870 nm | 870 nm | 870 nm | 1600 nm | 1600 nm | 1600 nm |
Location	Lat.	Lon.	T_{obs}	T_{noise}	T_8	T_{obs}	T_{noise}	T_8	T_{obs}	T_{noise}	T_8	T_{obs}	T_{noise}	T_8
CITIES														
London	51.44	-0.18	0.007	0.008	NaN	0.006	0.009	NaN	0.010	0.020	NaN	0.007	0.011	NaN
Paris	48.83	2.29	0.007	0.009	NaN	0.007	0.010	NaN	0.012	0.020	NaN	0.010	0.014	NaN
Mexico City	19.37	-99.15	0.013	0.017	NaN	0.014	0.021	NaN	0.012	0.015	NaN	0.012	0.016	NaN
Bombay	19.01	72.85	0.006	0.007	NaN	0.006	0.009	NaN	0.011	0.032	NaN	0.010	0.033	NaN
Beijing	39.85	116.40	0.005	0.005	NaN	0.006	0.007	NaN	0.006	0.007	NaN	0.005	0.005	0.001
CROPS														
Florida	27.36	-80.44	0.005	0.009	NaN	0.006	0.012	NaN	0.012	0.015	NaN	0.013	0.015	NaN
Lille,France	50.45	2.08	0.009	0.000	0.009	0.010	0.000	0.010	0.020	0.000	0.020	0.017	0.000	0.017
Netherlands	52.88	6.07	0.008	0.007	0.004	0.008	0.007	0.004	0.021	0.026	NaN	0.013	0.011	0.007
Milan,Italy	45.24	9.28	0.014	0.006	0.012	0.015	0.009	0.012	0.023	0.022	0.006	0.017	0.011	0.013
NSW,Australia	-35.43	146.93	0.005	0.004	0.004	0.009	0.006	0.006	0.015	0.013	0.008	0.013	0.010	0.009
TREES														
Finland	69.14	25.41	0.013	0.006	0.011	0.012	0.006	0.011	0.019	0.013	0.015	0.012	0.008	0.008
Para,Brazil	1.22	-56.90	0.008	0.011	NaN	0.008	0.010	NaN	0.015	0.020	NaN	0.011	0.014	NaN
DR Congo	1.58	28.29	0.010	0.000	0.010	0.010	0.000	0.010	0.018	0.000	0.018	0.013	0.000	0.013
Mekong,Cambodia	13.26	105.56	0.008	0.006	0.006	0.007	0.006	0.004	0.011	0.010	0.003	0.008	0.007	0.004
Amazonas,Brazil	-5.87	-58.36	0.011	0.012	NaN	0.010	0.010	NaN	0.016	0.017	NaN	0.013	0.013	NaN
MOUNTAINS														
Morocco	32.13	-5.12	0.009	0.010	NaN	0.008	0.010	NaN	0.008	0.011	NaN	0.008	0.011	NaN
Peru	-14.05	-73.18	0.009	0.015	NaN	0.009	0.016	NaN	0.014	0.032	NaN	0.014	0.032	NaN
Ben Nevis	56.74	-4.95	0.014	0.024	NaN	0.014	0.025	NaN	0.023	0.039	NaN	0.020	0.024	NaN
China (mountains)	25.84	101.38	0.006	0.007	NaN	0.006	0.008	NaN	0.010	0.012	NaN	0.008	0.010	NaN
Ethiopia	11.29	38.45	0.005	0.006	NaN	0.005	0.007	NaN	0.008	0.009	NaN	0.006	0.008	NaN
DESERT														
Libya	24.94	12.46	0.003	0.018	NaN	0.004	0.027	NaN	0.006	0.033	NaN	0.007	0.024	NaN
Algeria	30.78	8.13	0.003	0.002	0.003	0.005	0.003	0.003	0.006	0.004	0.004	0.008	0.004	0.006
Saudi Arabia	20.27	50.83	0.003	0.001	0.002	0.004	0.002	0.004	0.005	0.002	0.005	0.006	0.003	0.005
China (desert)	39.94	101.79	0.006	0.006	0.002	0.006	0.008	NaN	0.006	0.009	NaN	0.008	0.010	NaN
Namibia	-24.38	15.16	0.002	0.003	NaN	0.002	0.004	NaN	0.003	0.004	NaN	0.003	0.005	NaN
SNOW														
Greenland	73.99	-39.16	0.022	0.021	0.007	0.026	0.023	0.012	0.028	0.024	0.015	0.014	0.009	0.011
Antarctica (i)	-70.46	137.46	0.018	0.006	0.017	0.020	0.006	0.019	0.021	0.007	0.020	0.017	0.004	0.017
W.Greenland	70.30	-46.45	0.018	0.011	0.014	0.022	0.013	0.018	0.026	0.014	0.023	0.014	0.004	0.014
Svalbard	79.74	24.07	0.034	0.020	0.028	0.042	0.024	0.034	0.052	0.027	0.044	0.019	0.007	0.018
Antarctica (ii)	-79.53	23.61	0.017	0.009	0.015	0.023	0.011	0.020	0.028	0.013	0.025	0.023	0.005	0.022

Table 4: Table of variabilities for each location at each wavelength. The T_8 errors given here are calculated using Equation 1 (NaN indicates where the noise is greater than the observed variability). They are then averaged for each surface type, then the loosest error plus one standard deviation was selected for each category (snowy, vegetated and bare) and divided by $\sqrt{2}$ to give the actual T_8 values used in the new retrieval, listed in Table 2.
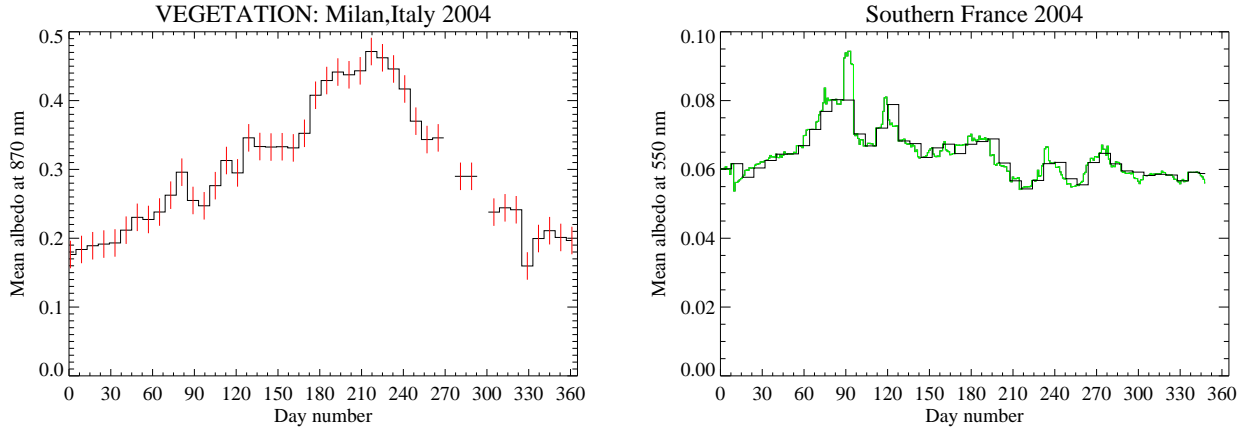
Figure 7: Examples of time-series over vegetation. The left-hand plot shows the 8-day mean albedos over Milan, Italy for 2004 with error bars of 0.02 marked in red. The phenological cycle is clearly seen, with green-up causing the annual increase in reflectance at 870 nm which lasts through the summer. The right-hand plot shows 550 nm albedo data reported daily (but still using a running mean over 16 days) for a vegetated area in Southern France (in green) along with the 8-day means (in black) for comparison. The daily albedo varies linearly and general trends are represented by the 8-day means but there can still be significant differences between the albedo value for a particular day and the 8-day mean for that period, such as around Day 90. Since these daily data are averages (MODIS cannot provide absolute albedo measurements every day), they are already smoothed to some extent and so still mask some of the 'true' or 'real' variability discussed in this report.

CITIES	550 nm	660 nm	870 nm	1600 nm
550 nm	1	0.92 ±0.01	0.27 ±0.11	0.32 ±0.20
660 nm	0.92 ±0.01	1	0.23 ±0.13	0.37 ±0.20
870 nm	0.27 ±0.11	0.23 ±0.13	1	0.60 ±0.30
1600 nm	0.32 ±0.20	0.37 ±0.20	0.60 ±0.30	1
CROPS	550 nm	660 nm	870 nm	1600 nm
550 nm	1	0.96 ±0.05	0.53 ±0.26	0.12 ±0.50
660 nm	0.96 ±0.05	1	0.40 ±0.35	0.17 ±0.53
870 nm	0.53 ±0.26	0.40 ±0.35	1	0.12 ±0.22
1600 nm	0.12 ±0.50	0.17 ±0.53	0.12 ±0.22	1
TREES	550 nm	660 nm	870 nm	1600 nm
550 nm	1	0.94 ± 0.04	0.28 ± 0.18	0.17 ± 0.39
660 nm	0.94 ± 0.04	1	0.22 ± 0.19	0.14 ± 0.35
870 nm	0.28 ± 0.18	0.22 ± 0.19	1	0.47 ± 0.31
1600 nm	0.17 ± 0.39	0.14 ± 0.35	0.47 ± 0.31	1
MOUNTAINS	550 nm	660 nm	870 nm	1600 nm
550 nm	1	0.96 ± 0.04	0.62 ± 0.27	0.19 ± 0.49
660 nm	0.96 ± 0.04	1	0.59 ± 0.29	0.25 ± 0.48
870 nm	0.62 ± 0.27	0.59 ± 0.29	1	0.40 ± 0.46
1600 nm	0.19 ± 0.49	0.25 ± 0.48	0.40 ± 0.46	1
DESERT	550 nm	660 nm	870 nm	1600 nm
550 nm	1	0.60 ± 0.29	0.40 ± 0.39	0.00 ± 0.36
660 nm	0.60 ± 0.29	1	0.93 ± 0.04	0.49 ± 0.54
870 nm	0.40 ± 0.39	0.93 ± 0.04	1	0.60 ± 0.56
1600 nm	0.00 ± 0.36	0.49 ± 0.54	0.60 ± 0.56	1
SNOW	550 nm	660 nm	870 nm	1600 nm
550 nm	1	0.97 ± 0.00	0.88 ± 0.05	-0.04 ± 0.21
660 nm	0.97 ± 0.00	1	0.93 ± 0.07	-0.02 ± 0.22
870 nm	0.88 ± 0.05	0.93 ± 0.07	1	0.09 ± 0.27
1600 nm	-0.04 ± 0.21	-0.02 ± 0.22	0.09 ± 0.27	1

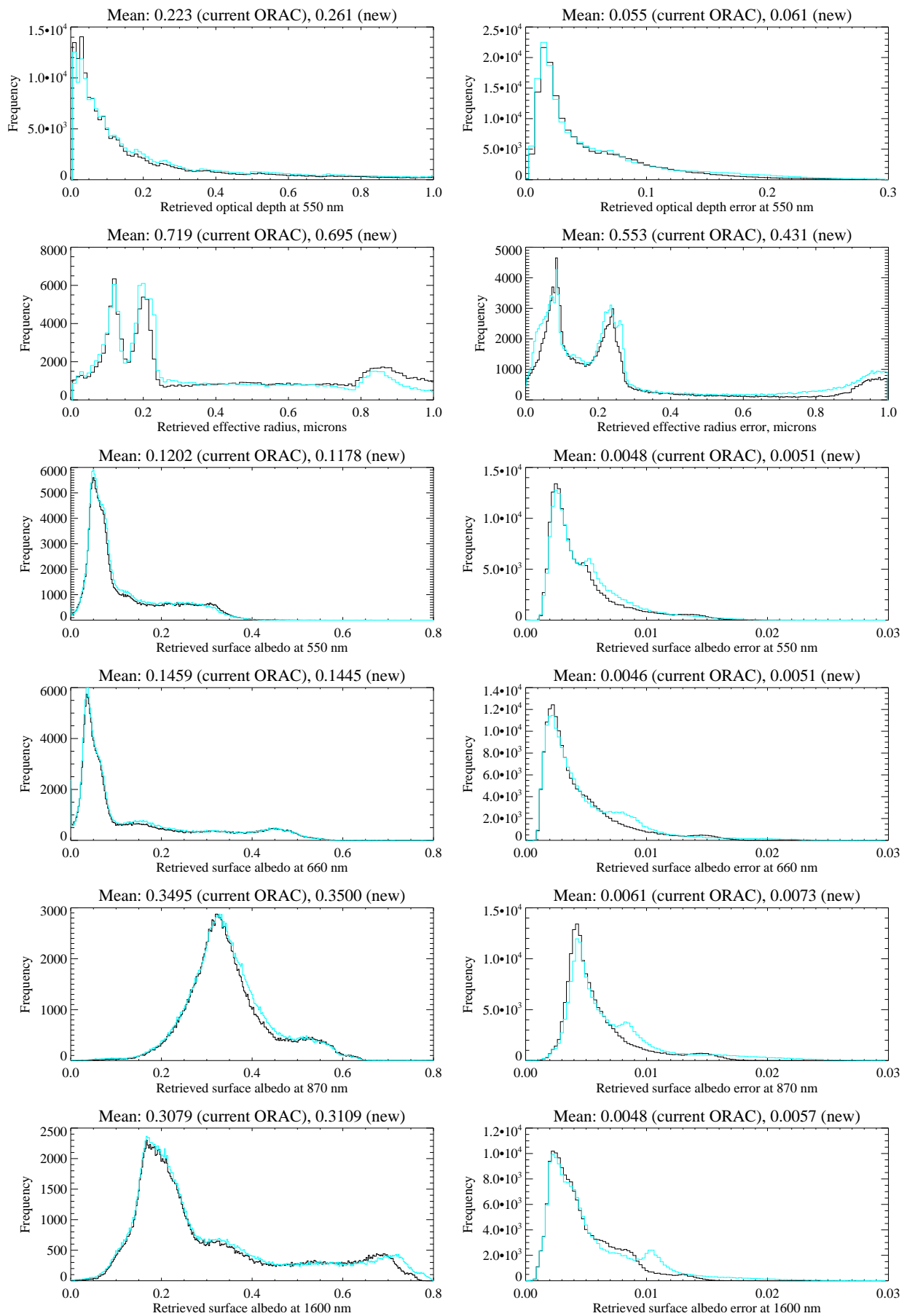Table 5: Correlation matrices for each surface type. Entries are of the form mean ± standard deviation.

Figure 8: Graphs of the retrieved aerosol parameters and their associated uncertainties. The results for the current ORAC retrieval are shown in black and the new retrieval in blue.